Ac conductivity in boron doped amorphous carbon films

*P. N. Vishwakarma**[a,b,c]

[a]*Department of Physics, Indian Institute of Science, Bangalore, India – 560012*

[b]*UGC-DAE Consortium for Scientific Research, University Campus, Khandwa Road, Indore, India-452017*

[c]*Department of Physics,NIT-Rourkela, Orissa, India-769008*

Published at : Solid State Communications 149 (2009) 115–120

(http://dx.doi.org/10.1016/j.ssc.2008.11.006)

Abstract: Experimental results on frequency and temperature dependence of ac conduction in boron doped graphite like amorphous carbon films are analyzed in the framework of available microscopic models. Depending on the response, the conductivity plot is divided into three regimes (low frequency high temperature; moderate frequency intermediate temperature; high frequency low temperature) and the data in the respective regimes are correlated to the various theoretical models accordingly. The conductivity data at high frequency and low temperature suggests that relaxation via quantum mechanical tunneling might be the dominant conduction mechanism. At intermediate temperatures and moderate frequencies, the conductivity data is in good agreement with extended pair approximation model with interaction correction. Signature of enhanced interaction effect in observed at low temperature.

PACS No: 71.30.+h, 72.20.-i, 72.60.+g , 72.80.Ng

Keywords: Disordered systems, thin films, ac conductivity, hopping conduction.

*email : prakash@csr.ernet.in, PrakashNath.Vishwakarma@nitrkl.ac.in

; FAX: +91 0731 2462294

1. INTRODUCTION

Amorphous carbon materials prepared by any means contains varying ratio of sp3 to sp2 bonded carbon atoms [1]. The physical and chemical properties of these carbon materials significantly depend on this ratio as sp3 carbon induces diamond like properties whereas sp2 bonded carbon induce graphite like properties [2]. Sometimes the microstructure of the amorphous carbon materials prepared using different techniques differs considerably for the same sp3/sp2 ratio. Since the conduction mechanisms in any carbon-based material are closely linked to the microstructure of the material, electrical conduction in disordered π-electron system is therefore of particular interest [3]. Though there are a number of amorphous carbon systems rich in π-bonded carbon atoms, here the discussion will be restricted to the amorphous carbon prepared using pyrolysis assisted CVD technique [4]. These amorphous carbons mostly contain sp2 bonded carbon atoms with negligible hydrogen content and reveal graphitic ordering on annealing at high temperature [5]. The electrical transport measurements on these amorphous carbon show metal insulator (M-I) transition, which can be linked to the change in microstructure on annealing temperature [6]. The effect of boron doping on the dc electrical transport properties in these amorphous carbons reveal low conductivity indicating fall in the density of conducting π-electrons with increasing boron content [7]. The conductivity in these samples follow Mott hopping conduction relation at low temperature with a

signature of crossover from Mott to Efros-Shklovskii hopping law for less conducting samples [8].

It has been debated for long that the ac and dc conduction in any disordered materials are closely related, hence investigation of ac conduction in addition to dc conductivity can provide more information of the electrical conduction [9]. Generally the ac conductivity data is analyzed only for the real part and is found to obey a power law in frequency and temperature, $\sigma \propto \omega^s T^n$ [10]. However we believe, the imaginary part can give better information on the phase dependence of ac signal and should always be included in the analysis. Hence the ac conductivity data for boron doped amorphous carbon films prepared using pyrolysis assisted CVD technique has been analyzed for real as well as imaginary part of the conductivity.

2. EXPERIMENTAL DETAILS

The boron doped amorphous carbon films are prepared using high temperature pyrolysis assisted CVD of carbon rich organic precursor under inert atmosphere. Standard solution of boric acid (H_3BO_3) in distilled water is used as the boron source [11] and maleic anhydride ($C_4H_2O_3$) as the organic precursor. Clean polished quartz pieces (5mm x 5mm x 1mm) are used as substrates to deposit these films. Details of preparation can be found somewhere else [5-7]. Boron concentration in the sample is altered by varying the initial concentration of boric acid in the solution (1M, ½ M, ¼ M). The atomic percentage of boron in these carbon films is found to be 25% (CB700M), 18% (CB700M2) and 10% (CB700M4). In our notation of the samples, for example

CB700M2, C and B stand for carbon and boron, 700 is the pyrolysis temperature in ^{0}C and M2 stands for half molar boric acid solution initially used.

AC conductivity for all the samples are measured from 1Hz to 102kHz in the temperature range of 300 K to 4.2 K using liquid helium cryostat supplied by Janis Corp, USA. The electrical contacts to the sample are made using conducting silver epoxy in accordance to standard four-probe technique. Impedance measurements are performed using SR 830 lock-in amplifier (Stanford Instruments). Lock-in amplifiers work on the principle of phase sensitive detection technique to single out the component of the signal at a specific reference frequency and phase, leaving the noise signals at frequencies other than reference frequency. Hence lock-in amplifiers can be effectively used for very accurate measurements even when the small signal is obscured by noise sources many thousands of times larger. Lock-in amplifier does not directly give the impedance value but it can be evaluated using the following relation.

$$Z = \frac{V_S}{I_S} = \frac{V_S}{V_R} \times R \tag{1}$$

$$= R \times \left(\frac{V_S' + jV_S''}{|V_R|} \right)$$

$$= R \times \left(\frac{V_S' + jV_S''}{\sqrt{(V_R')^2 + (V_R'')^2}} \right) \tag{2}$$

So,

$$Z' = R \times \frac{V_S'}{\sqrt{(V_R')^2 + (V_R'')^2}} \tag{3}$$

$$Z'' = R \times \frac{V_S''}{\sqrt{(V_R')^2 + (V_R'')^2}} \tag{4}$$

where V_S and V_R are the voltages across the sample and standard resistor R=100 ohm connected in series with the sample. The purpose of the standard resistor is to estimate the current passing through the sample, as lock-in amplifier does not give constant ac current. While calibrating the experimental setup (without sample), voltage drop across the standard resistor is found to be purely real ($V_R'/V_R'' > 10^3$), but due to sample effect a phase shift is introduced in the current flowing across the loop and this current having non-zero phase resulted an imaginary signal (in addition to the real) across the resistor. This imaginary signal across the resistor while sample is in the loop, is not due to resistor as no phase shift is introduced by the resistor. The magnitude of the current flowing in the loop is proportional to the modulus of the voltage drop across the resistor, as the phase shift has already been accounted while sampling the imaginary part of sample voltage.

3. RESULTS AND DISCUSSION

Prior to structural analysis, the boron doped amorphous carbon samples are examined for hardness test using Shimadzu Microhardness Tester. Boron doped samples are found to be more brittle than the undoped one and making good indentation on them was a challenging task. Maximum hardness (1400 kg/mm^2) is found in undoped amorphous carbon and gradual decrease in hardness with increasing boron content is observed (1100 kg/mm^2 for CB700M4 and 750 kg/mm^2 for CB700M2). The sample with maximum boron content (CB700M) was too soft and brittle to make any good indentation; hence hardness value is not evaluated. Decreasing hardness of the boron

doped amorphous carbon films rules out the presence of crystalline boron carbide or any such hard phase in the sample.

The surface morphology of the boron doped amorphous carbon films are analyzed using scanning electron microscopy (SEM). The SEM images of the boron doped carbon films are compared with those of undoped films (Fig. 1). The undoped GAC film is very smooth except few island like structures projecting outward (right hand side corner of the image). Very few such islands were observed on the surface. With the incorporation of boron in the carbon network, the density of these nucleating islands increases and projects further to form spherical balls (CB700M4). Further increment in boron content, i.e. CB700M2 and CB700M, increases the density as well as the size of these microscopic balls. The average size of these balls in CB700M2 is $\sim 0.5\mu m$, whereas for CB700M, it grows upto $\sim 1.5\mu m$. At present the exact nature of these nucleating balls is not very clear. Further microstructural details of these samples can be found in ref [7, 8]

The classification of the samples is done using reduced activation energy 'W' ($W(T) = -\partial(\log\rho)/\partial(\log T)$ plots, as suggested by Zabrodskii [12]. According to this scheme the slope of W versus T in log-log scale is positive (inset of fig 2) which is an indication of sample lying in the insulating side of M-I transition boundary. The dc conductivity data in these samples is well explained by variable range hopping (VRH) conduction through localized states, $\ln[\rho(T)] \propto T^{-x}$, where x = ¼ for Mott VRH and x = ½ for ES VRH (fig2) [13, 14]. The temperature dependence of resistivity for C700 shows a good fit for x = 0.25 at low temperature and x = 0.16 at high temperature. The corresponding temperature exponents for CB700M4 varies from x = 0.20 at room temperature to 0.36 at low temperature via 0.25 at intermediate temperatures. Similar

values of ‘x’ were observed for CB700M2 except, at low temperature where the exponent was found to be 0.45. Since x = 0.5 is an indication of ES hopping, it seems that at low temperature, transition from Mott VRH (x = 0.25) to ES VRH (x = 0.5) is taking place. For CB700M4, the exponents increases from x = 0.25 to 0.36 but it has not yet reached x = 0.5. Probably for this sample, still lower temperature is required to observe ES VRH. In C700 no cross over is observed even for lowest temperature. D.c conductivity and magnetoresistance data on these films indicate transition from Mott to Efros-Shklovskii VRH at low temperatures [8].

The ac conductivity measurements are carried out on each sample at various temperatures (at frequencies 1kHz, 10kHz, 50kHz and 100kHz) and at different frequencies (keeping temperature constant at 4.2 K, 31 K, 77 K and 300 K). The frequency and temperature dependence of ac conductivity for least doped CB700M4 and highly doped CB700M amorphous carbon films are shown in Fig. 3 and Fig. 4. For the sake of conciseness, results for all other samples along with CB700M2 and C700 are summarized in table I and II. The ac conductivity for all the samples in general can be shown to have behaviour as in Fig. 5. In the plot, only the magnitude of imaginary part of the conductivity is plotted. In actual case the imaginary part of conductivity will be lagging behind the real part by a phase difference determined by the sample and hence will be in negative scale.

The macroscopic technique adopted by Dyre and Schroder [15] has got lot of attention in understanding the ac conductivity behaviour in disordered solids. However group IV elements have been exception to this model and the ac conductivity behaviour of this group of materials is still under debate. So the analysis of the conductivity data has

been done using microscopic models. Depending upon the response, the conductivity plot has been divided into three regimes and each regime has been discussed separately (Fig. 5).

A. Regime I

At low frequencies and high temperatures, the conductivity value is roughly the same as the dc conductivity. In this time scale (inversely proportional to the applied frequency), the electric field acting on the carrier electrons is not able to perturb the dc conduction mechanism. The electrons see a uniform electric field during the time of flight, hence the conductance is the dc value. As the frequency is increased further the conductivity does not change until a critical frequency or temperature beyond which the conductivity increases slowly but nonlinearly. The microscopic model for ac conductivity is applicable only beyond this regime.

B. Regime II

In this regime the frequency dependence of the real part of conductivity in log scale increases linearly with slope nearly equal to two, $s' \approx 2$. Such quadratic dependence of conductivity on frequency is considered as breakdown of pair-approximation. It is assumed that at high frequency, the relaxation is confined entirely to pairs of sites, and multiple site participation is excluded. However, the pair approximation has been found to be good only at sufficiently high frequencies and breaks down at low frequencies, where a percolation path must be established throughout the sample in the dc limit. Butcher and coworkers developed a so-called “extended pair approximation” (EPA) [16-18] in which the effect on the relaxation rate for a given pair of sites of all the other sites in the network is taken into account in an averaged way. This effect is neglected in pair

approximation where the hopping or tunneling is restricted to a pair of potential wells. Using EPA approach, the correction to the real part of ac conductivity at low frequency is found to be proportional to ω^2 i.e, $s' = 2$ [19, 20]. So the quadratic behaviour of conductivity in frequency for these samples can be explained using EPA approach.

The temperature exponent of the real part of conductivity, n', is found to be negative in this regime. The observed value of slope (n') for C700 is $n' \approx -2.6$, which drift towards $n' \approx -1$ with increasing boron content in the carbon network (see table II). To the best of our literature survey, we have not come across any microscopic model on electronic system, which predicts such temperature dependence. Recently while dealing with ionic conductivity, Murugavel et.al proposed that in the absence of interaction, the temperature exponent at low frequency should be proportional to $T^{-2.3}$ i.e $n' = -2.3$ and shifts to $n' = -1$, for strong interaction in the system [21, 22]. Baranvoskii and Cordes carried out analytical calculations on the dynamics of a single particle using a percolation approach and found the temperature exponent to be -2.3 [23]. This analytical result is also qualitatively confirmed by recent computer simulations carried out by Schroder and Dyre [15, 24]. Though it is not clear how the ionic conductivity model can explain conduction in electronic systems, but the experimental observations on these samples indicates that the excitations giving rise to ac conduction in ionic and electronic systems in this regime are closely related.

The imaginary part of conductivity in this regime is found to be having frequency exponent $s'' \approx 1.8$ and temperature exponent varies from $n'' \approx -4.5$ to $n'' \approx -1$. So far we have not come across any theoretical model, which predicts such temperature dependence and frequency dependence for the imaginary part of conductivity. Hence at present it is

difficult to comment more about the conduction mechanism responsible for such behaviour of the imaginary part of conductivity.

C. Regime III

As the frequency is increased, i.e. when the pair approximation is approached, $\sigma(\omega)$ changes from ω^2 dependence to ω dependence. Such roll-off behaviour at high frequencies has also been observed in amorphous Si and Ge [25]. The conductivity dependence on frequency looks almost linear with $s' \approx 1.05$. Similar value of '$s' \approx 1.05$' has also been observed in few other materials [26-28]. One such model, which proposes superlinear frequency exponent is, relaxation via tunneling when interactions among the electrons are dominant [25, 29, 30] and can be written as,

$$\sigma'(\omega) \propto \omega^{s'}; \text{ where } s' = 1 + \frac{1}{\ln(1/\omega\tau_{0t})} \quad (5)$$

$$\sigma''(\omega) \propto \omega^{s''}; \text{ where } s'' = 1 \quad (6)$$

and the corresponding temperature exponent,

$$n' = n'' = 0 \quad (7)$$

In terms of microscopic theory, the exciting field changes the relative environment of a pair of centers and causes transition between them governed by the intrinsic relaxation time τ of the pair. The resultant loss is dominated by pairs having relaxation times τ around ω^{-1}. So in the limit of high frequency, transitions are taking place mostly from those sites for which relaxation times are very small i.e. only from neighbouring sites. Since the frequency dependence of imaginary part of conductivity is same in regime II and III, same discussions will be retained for regime III except for the highly resistive

samples, which show a change in slope after reaching a maximum value at high frequency. Such behaviour has also been observed in disordered ionic solids but the phenomenon responsible for this is still not clear [31].

According to the microscopic model predictions, the real as well as imaginary conductivity should show temperature independent conductivity [eq. (7)]. The most striking feature of the ac conductivity in this regime is the lack of temperature dependence at the lowest temperatures $n' \approx 0$ for the real as well as the imaginary part of conductivity. This is a clear indication of relaxation via quantum mechanical tunneling in the presence of interaction.

4. CONCLUSIONS

The ac conductivity in boron doped amorphous carbon films follows the universal power law and is in proximity with microscopic model. At low temperature and high frequency, the real part of conductivity shows super-linear frequency exponent and almost no temperature dependence. This is a clear indication of relaxation via quantum mechanical tunneling. Though the temperature independent imaginary part of conductivity is in agreement with microscopic model, quadratic frequency dependence is not yet understood. At intermediate temperature and moderate frequencies, the ac conductivity data is in accordance to the extended pair approximation model for ionic conductors. This indicates that the excitations leading to ac conduction in both ionic and these systems might be having similar origin. However further investigations are required to draw any conclusions.

AKNOWLEDGEMENTS

Acknowledgement is due to Dr. P. Chaddah, Prof. Ajay Gupta and Dr. V. Ganesan for their encouragement and support. My sincere thanks Prof. S.V. Subramanyam for helpful discussions and Dr. S. Sarangi for discussions regarding the experiment.

References:

1. S. R. P. Silva, J. D. Carey, R. U. A. Khan, E. G. Gerstner and J. V. Anguita, in Hand book of Thin film Materials, edited by H. S. Nalwa, (Academic press, New York, 2002) Vol.4, p-403

2. J. Robertson, Mater. Sci. Eng. R, 37 (2002) 129

3. K. Shimakawa and K. Miyake, Phys. Rev. B 39, (1989) 7578; D. Dasgupta, F. Demichelis and A. Tagliaferro, Phil. Mag. B 63, (1991) 1255; A. Helmbold, P. Hammer, J. U. Thiele, K. Rohwer and D. Meissner, Phil. Mag. B. 72 (1995) 335

4. V. Meenakshi and S. V. Subramanayam, J. Appl. Phys. 92 (2002) 137

5. P. N. Vishwakarma, V. Prasad, S. V. Subramanyam and V. Ganesan, Bull. Mater. Sci. 28, (2005) 609

6. V. Prasad and S. V. Subramanyam, Physica B 369, (2005) 168

7. P.N.Vishwakarma and S.V.Subramanyam, Phil. Mag. 87, (2007) 811

8. P.N.Vishwakarma and S.V.Subramanyam, J.Appl. Phys. 100, (2006) 113702

9. E. Helgren, G. Grüner, M. R. Ciofalo, D. V. Baxter and J. P. Carini, Phys. Rev. Letts. 87, (2001) 116602

10. A. K. Jonscher, Nature 267 (1977) 673; S. R. Elliott, Physics of Amorphous Materials 2nd ed. (Longman scientific and Technical, London, 1990)

11. J. T. Huang, W. H. Guo, J. Hwang and H. Chang, Appl. Phys. Letts. 68 (1996) 3784

12. A. G. Zabrodskii, Sov. Phys. Semicond. 11, (1977) 345

13. N. F. Mott and E. A. Davis, Electronic process in non-crystalline materials. (Clarendon press, Oxford, 1971)

14. A. L. Efros and B. I. Shklovskii, Electron-Electron interactions in Disordered Systems, edited by A.L.Efros and M.Pollak (Amsterdam, North-Holland, 1985)

15. J. C. Dyre and T. B. Schroder, *Rev. Mod. Phys.* 72 (2000) 873

16. P. N. Butcher and S. Summerfield, *J. Phys. C* 14 (1981) L1099

17. S. Summerfield and P. N. Butcher, *J. Phys. C* 15 (1982) 7003

18. S. Summerfield and P. N. Butcher, *J. Phys. C* 16 (1983) 295

19. S. Summerfield and P. N. Butcher, *Phil. Mag. B* 49 (1984) L65

20. S. Summerfield, *Phil. Mag. B* 52 (1985) 9

21. S. Murugavel and B. Roling, *Phys. Rev. Lett.* 89 (2002) 195902

22. B. Rolling, *Phys. Chem. Chem. Phys.* 3 (2001) 5093

23. S. D. Baranovskii and H. Cordes, *J. Chem. Phys.* 111 (1999) 7546

24. T. B. Schroder and J. C. Dyre, *Phys. Rev. Lett.* 84 (2000) 310

25. A. R. Long, *Adv. Phys.* 31 (1982) 553

26. R. B. South and A. E. Owen, *Proc. 5th Int. Conf. on Amorphous and Liquid Semiconductors*, edited by J. Stuke and W. Brenig (Taylor & Francis, London, 1974)

27. J. J. Hauser, *Solid St. Commun.* 50 (1984) 623

28. J. J. Hauser, *Phys. Rev. B* 31 (1985) 2133

29. S. R. Elliott, *Adv. Phys.* 36 (1987) 135

30. J. J. Hauser, *Phys. Rev. Lett.* 44 (1980) 1534

31. W. Dieterich and P. Maass, *Chem. Phys.* 284 (2002) 439

Table 1
The frequency exponents for all the samples in various frequency ranges.

Temp		C700 s(range in kHz)	CB700M4 s(range in kHz)	CB700M2 s(range in kHz)	CB700M s(range in kHz)
4.2 K	s'	1.97 (0.3–1.1)	2.1 (3–12)	1.95 (0.1–0.5)	1.96 (0.1–0.3)
		1.02 (> 1.1)	1.01 (> 12)	1.07 (> 0.5)	1.04 (> 0.3)
	s''	1.83 (> 0.5)	1.83 (> 0.4)	1.81 (> 0.2)	1.84 (> 0.1)
31 K	s'		2.06 (10–30)	1.97 (3–15)	2.01 (0.3–1)
			1.35 (> 30)	1.05 (> 15)	1.03 (> 1)
	s''		1.84 (> 10)	1.85 (> 9)	1.88 (> 0.2)
77 K	s'		2.05 (> 25)	1.98 (7–25)	2.06 (1–4)
			–	1.05(> 25)	1.04 (> 4)
	s''			1.83 (> 20)	1.85 (> 0.7)

Table 2
The temperature exponents for all the samples in various temperature ranges.

Freq		C700 n (range in K)	CB700M4 n (range in K)	CB700M2 n (range in K)	CB700M n (range in K)
1 kHz	n'	0.5 (< 17)	–	0.003 (< 9)	0.01 (< 15)
		−2.8 (17–25)	–	−1.6 (9–24)	−2 (15–83)
	n''	–	–	–	0.06 (< 7)
		−4.4 (< 22)	–	−3.1 (< 15)	−2.1 (7–46)
10 kHz	n'	0.1 (< 30)	0.07 (< 17)	0.06 (< 20)	0.03 (< 52)
		−2.7 (30–60)	−1.3 (17–39)	−1.05 (20–95)	−1.5 (52 – 300)
	n''	–	0.03 (< 17)	–	0.02 (< 12)
		−4.5 (< 42)	−1 (17–28)	−2.7 (< 55)	−1.7 (12–215)
50 kHz	n'	0.05 (< 60)	0.004 (< 27)	0.03 (< 57)	0.02 (< 161)
		−2.6 (60–150)	−1.5(27–131)	−1 (57–300)	–
	n''	–	0.02 (< 18)	0.1 (< 7)	0.05 (< 19)
		−3.5 (< 101)	−1.4 (18–85)	−1.8 (7–300)	−1.3 (19–300)
100 kHz	n'	0.02 (< 90)	0.02 (< 46)	0.03 (< 112)	0.02 (< 261)
		−2.6 (90–160)	−1.6 (46–235)	−1(112–300)	–
	n''	0.5 (< 16)	0.04 (<19)	0.08 (< 10)	0.03 (< 22)
		−3 (16–163)	−1.4 (19–128)	−1.4 (10–300)	−1.1 (22–300)

FIGURE CAPTIONS

FIG. 1. Surface morphology of C700, CB700M4, CB700M2 and CB700M films using scanning electron microscope.

FIG. 2 Temperature dependence of resistivity for samples CB700M2, CB700M4, C700. The numerals depicted against the linear fitting denote the temperature exponent 'x' in the respective temperature range. CB700M was too resistive to carry out any dc resistivity measurements. The inset shows the Zabrodskii plot indicating insulating nature of the C700 and CB700M4 samples.

FIG. 3. (a) Plot of real and imaginary part of ac conductivity (a) as a function of frequency at different temperatures. (b) as a function of temperature at various frequencies along with dc conductivity for CB700M4 films. The solid symbols are for real part of conductivity and the open symbols for imaginary part of conductivity.

FIG. 4. Plot of real and imaginary part of ac conductivity (a) as a function of frequency at different temperatures. (b) as a function of temperature at various frequencies along with dc conductivity for CB700M films. The solid symbols are for real part of conductivity and the open symbols for imaginary part of conductivity. Inset in (a) shows the magnified view of same with additional plot corresponding to $s' = 1$.

FIG. 5. General behaviour of the observed ac conductivity as a function of (a) frequency and (b) temperature, for boron doped GAC films. The conductivity plot is divided into various regimes as discussed in the text. The observed frequency and temperature exponents are also labeled in the respective regimes.

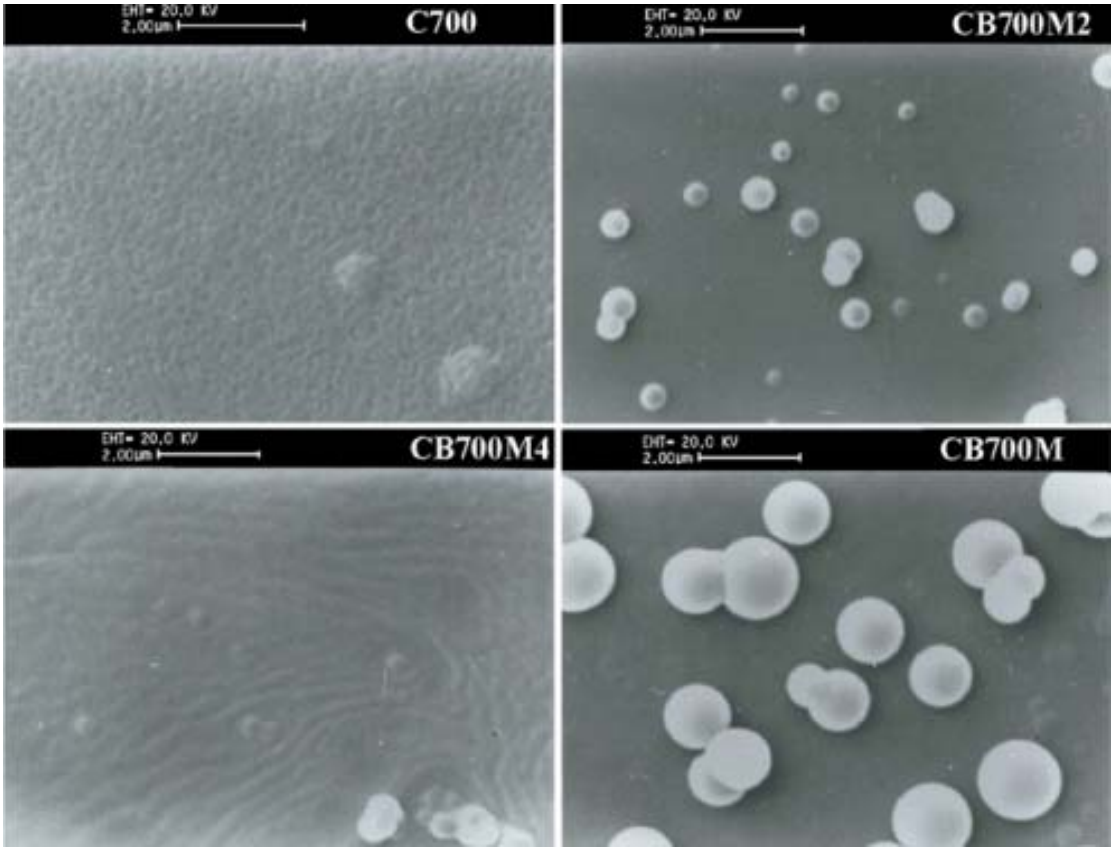

Figure 1 Surface morphology of C700, CB700M4, CB700M2 and CB700M films using scanning electron microscope

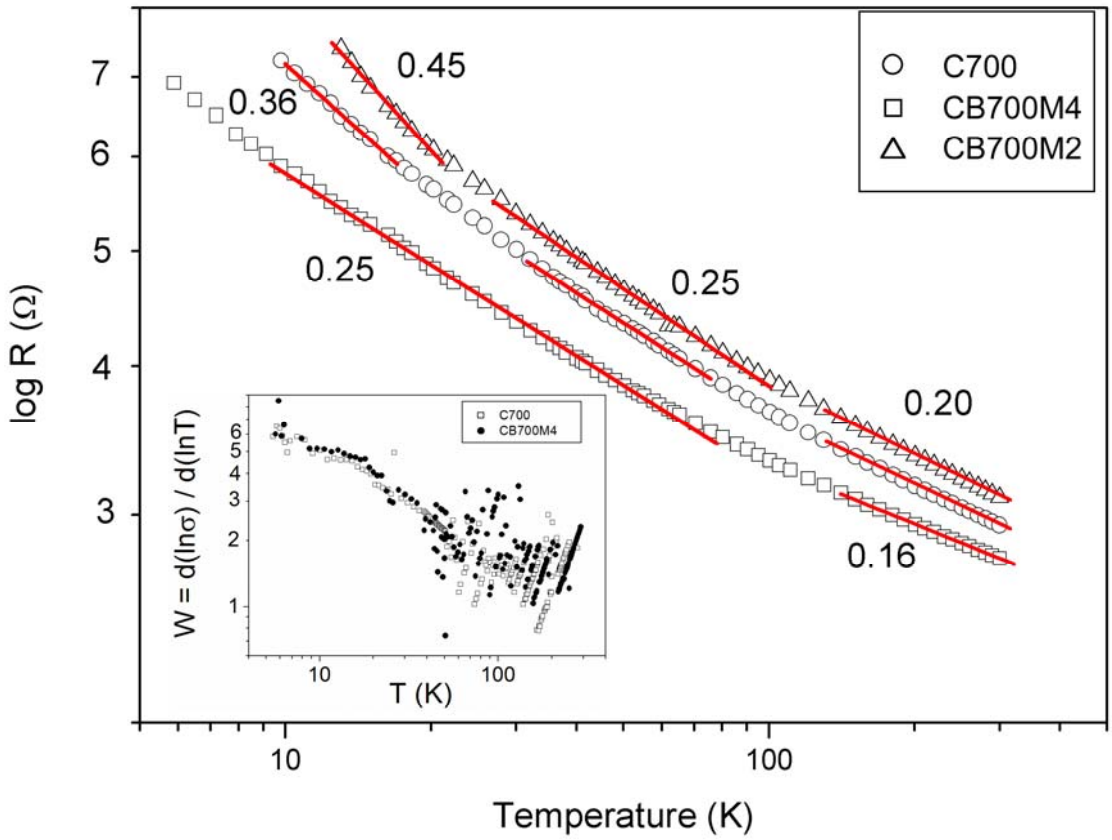

Figure 2. Temperature dependence of resistivity for samples CB700M2, CB700M4, C700. The numerals depicted against the linear fitting denote the temperature exponent 'x' in the respective temperature range. CB700M was too resistive to carry out any dc resistivity measurements. The inset shows the Zabrodskii plot indicating insulating nature of the C700 and CB700M4 samples

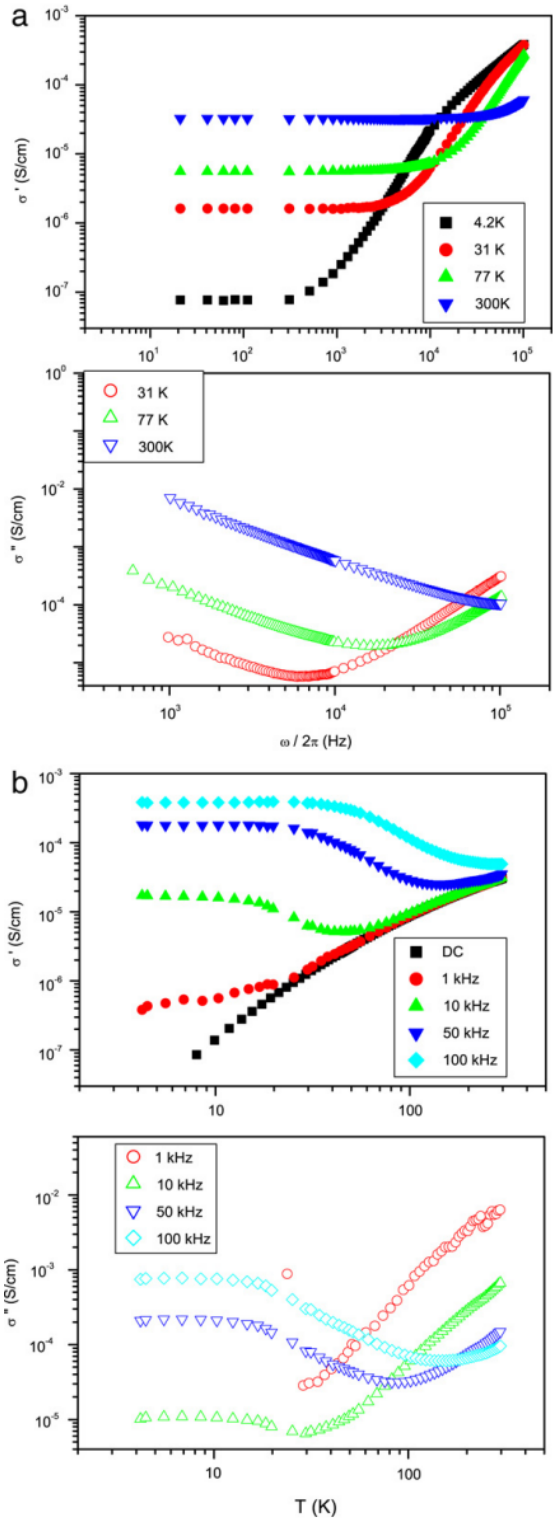

Figure 3. Plot of real and imaginary part of ac conductivity (a) as a function of frequency at different temperatures. (b) as a function of temperature at various frequencies along with dc conductivity for CB700M4 films. The solid symbols are for real part of conductivity and the open symbols for imaginary part of conductivity.

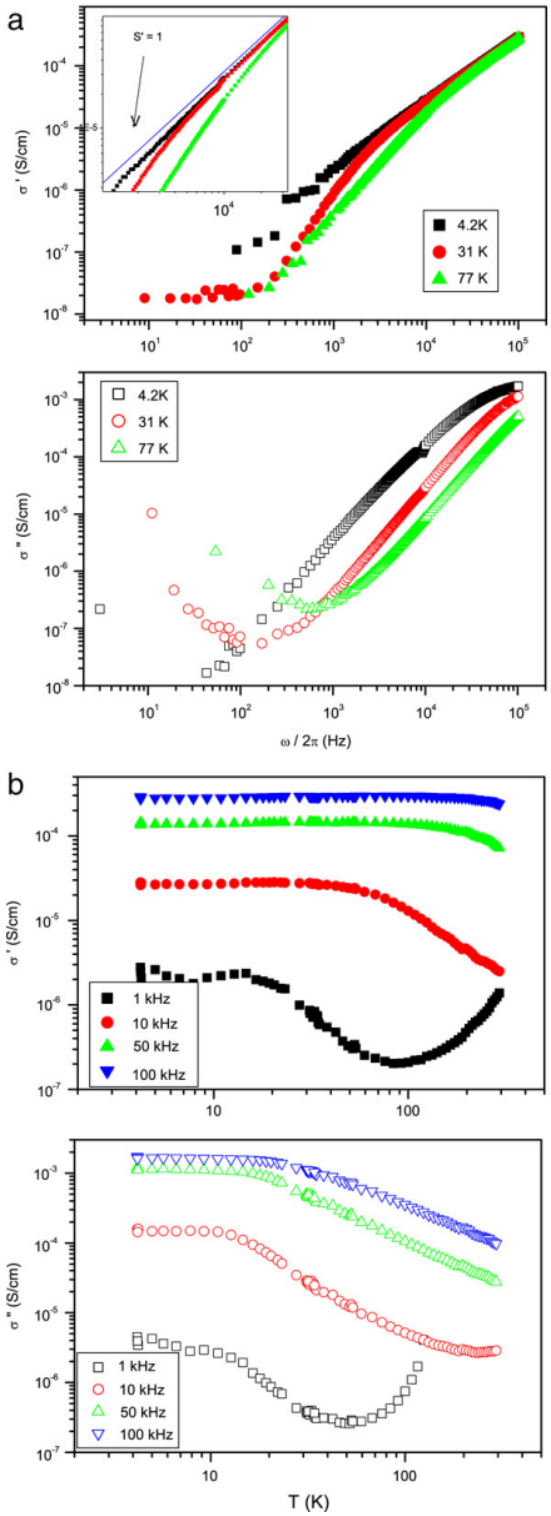

Figure 4. Plot of real and imaginary part of ac conductivity (a) as a function of frequency at different temperatures. (b) as a function of temperature at various frequencies along with dc conductivity for CB700M films. The solid symbols are for real part of conductivity and the open symbols for imaginary part of conductivity. Inset in (a) shows the magnified view of same with additional plot corresponding to s' = 1

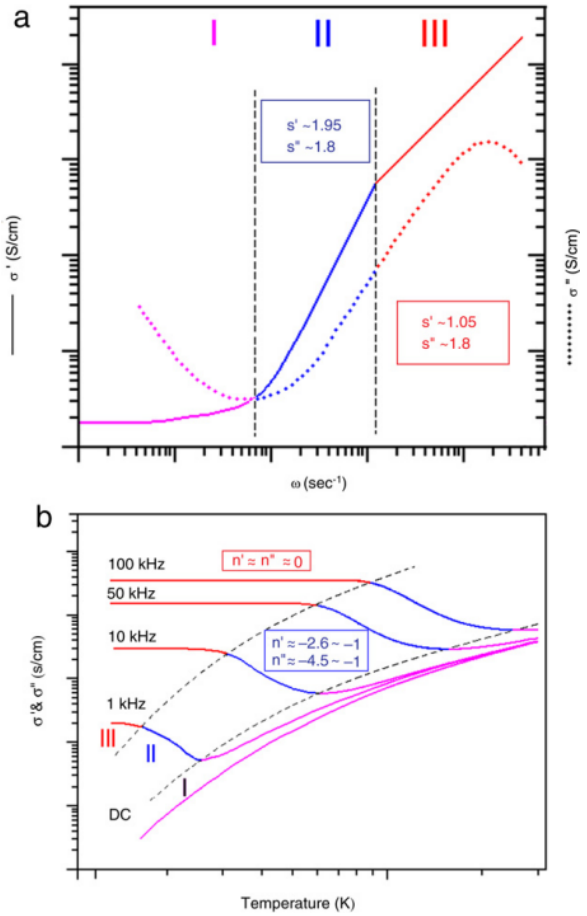

Figure 5. General behaviour of the observed ac conductivity as a function of (a) frequency and (b) temperature, for boron doped GAC films. The conductivity plot is divided into various regimes as discussed in the text. The observed frequency and temperature exponents are also labeled in the respective regimes